ASME Open Journal of Engineering
Online journal at:
https://asmedigitalcollection.asme.org/openengineering

M. Rifat Hasan Rubel
Applied Mathematics Department,
University of Dhaka,
Dhaka 1000, Bangladesh
e-mail: rifathrubel@gmail.com

M. Ferdows[1]
Applied Mathematics Department,
University of Dhaka,
Dhaka 1000, Bangladesh
e-mail: ferdows@du.ac.bd

Tahia Tazin
Department of Mathematics,
Comilla University,
Comilla 3506, Bangladesh
e-mail: tahiatanuja30@gmail.com

T. A. Bég
Engineering Mechanics Research,
Israfil House,
Dickenson Road,
Manchester M13, UK
e-mail: tasveerabeg@gmail.com

O. Anwar Bég
Multi-Physical Engineering Sciences Group,
Mechanical Engineering Department,
School of Science,
Engineering and Environment (SEE),
University of Salford,
Manchester M54 WT, UK
e-mail: O.A.Beg@salford.ac.uk

Ali Kadir
Multi-Physical Engineering Sciences Group,
Mechanical Engineering Department,
School of Science,
Engineering and Environment (SEE),
University of Salford,
Manchester M5 4WT, UK
e-mail: a.kadir@salford.ac.uk

Computation of Stagnation Point Convection Flow of Carbon Nanotube Nanofluids From a Stretching Sheet With Melting: *Dual Solutions*

A theoretical study in stagnation point flow is presented where melting heat transfer effects of carbon nanotube (CNT) from a stretching surface is appeared. Both carbon nanotubes like single-wall CNT (SWCNT) and multiwall CNT (MWCNT) are homogeneously dispersed in the base fluid. As the ordinary (or base) fluids, water and kerosene oil are employed. A set of nonlinear ordinary differential equations with appropriate boundary conditions is formed by transforming the governing equations via similarity transformations. The transformed nonlinear ordinary differential equations are then solved numerically using the bvp4c solver in MATLAB*, an efficient numerical finite difference method. The impact of nanoparticle volume fraction, velocity, melting, stretching parameter, and CNT type on transport characteristics are explored and visualized graphically and in tabular forms. Verification of the* MATLAB *computations with available data in certain limiting cases is included showing excellent agreement. Existence of dual (upper and lower branch) solution is shown for a certain range of stretching sheet parameter. The obtained dual solutions are examined for velocity and temperature in detail. A stability analysis demonstrates that the first solution is a stable solution, and the second solution is an unstable solution. Local skin friction and local Nusselt number are also computed in order to determine critical values that can permit dual solutions. It is observed that when a dimensionless melting parameter is greater than 1, SWCNT nanofluids attain greater velocities than MWCNT nanofluids for water as well as kerosene oil base fluids. Moreover, the flow is accelerated for SWCNT compared with MWCNT for both water and kerosene oil. With increasing stretching parameter, the heat transfer rate (Nusselt number) increases, whereas skin friction coefficients decrease. Higher skin friction and Nusselt number are obtained for SWCNTs compared to MWCNTs due to their greater density and thermal conductivity. The study is relevant to phase change manufacturing fluid dynamics of nanomaterials.* [DOI: 10.1115/1.4063645]

Keywords: stagnation flow, CNT nanofluids, melting heat transfer, similarity upper and lower branch solutions, stretching sheet, MATLAB, analytical methods of heat transfer, applied mechanics simulation, fluid flow, heat transfer, nanoscale heat transfer

1 Introduction

Boundary layer convective heat transfer from a stretching sheet arises in a diverse range of industrial applications such as coating processes, polymer manufacture, cooling and drying of paper, and so on. Many applications of such flows are reviewed in Vajravelu and Mukhopadhyay [1] including polymer extrusion, coating deposition, surficial finishing, and thin film fabrication. The boundary layer flow over a continuous stretching surface was first analyzed by Sakiadis [2,3]. Crane [4] later derived exact solutions for flow and heat transfer from a linearly stretching plate. Plane stagnation point flow (also known as the Hiemenz flow) also features extensively in materials synthesis operations. Both stretching and stagnation flows have stimulated extensive interest in applied mathematics and engineering analysis. Liancun et al. [5] studied the presence of nonuniform heat source/sink to investigate the unsteady flow and heat transfer over a permeable stretching sheet. Anwar Bég et al. [6] analyzed heat transfer characteristics in stagnation point flow toward a stretching sheet, observing that the free-stream velocity exceeds the stretching velocity and generates a boundary layer, whereas an inverted boundary layer is produced when this case is reversed. Anwar Bég et al. [7] deployed the

[1]Corresponding author.

Manuscript received November 9, 2022; final manuscript received September 11, 2023; published online November 6, 2023. Assoc. Editor: Oleg Schilling.

electrothermal network simulation to compute the momentum and heat transfer characteristics from a vertical translating surface adjacent to thermally stratified Darcy–Forchheimer porous media. Numerous other stagnation flow investigations have also been reported for both Newtonian viscous and non-Newtonian fluids. These include the studies by Gupta et al. [8] (on hydromagnetic micropolar plane stagnation flow), Ishak et al. [9] (on mixed convection Newtonian flow), Anwar Bég et al. [10] (on plane stagnation thermosolutal convection flow of micropolar fluids impinging on a cylinder), Ramesh et al. [11] (on two-phase magnetio-convective stagnation flow from a porous stretching surface), and Mehmood et al. [12] (on nonorthogonal reactive magneto-viscoelastic convection with thermal relaxation effects).

In recent years, the science of *nanofluid mechanics* has been developed extensively. A nanofluid is a colloidal fluid comprising nanometer-sized particles (diameter <50 nm), i.e., nanoparticles suspended in a viscous base fluid [13]. Nanofluids can increase effective thermal conductivity of conventional base fluids for the improvement of heat transfer rates. Base fluids such as water, oil, and ethylene glycol are popular in the design of nanofluids that have found extensive use in materials processing, energy science, and also biomedical systems [14]. Choi and Eastman [15] have provided a detailed appraisal of the excellent thermal properties of nanofluids and shown that either *nanoparticles* or *nanotubes* can be suspended in the base fluids. Choi et al. [16] have shown experimentally and theoretically that the thermal conductivity can be enhanced to 10–50% of heat transfer fluids, even with small solid volume fraction of nanoparticles (normally <5%). These findings have been confirmed in many other subsequent investigations including the studies by Masuda et al. [17], Das et al. [18], Pak and Cho [19], Xuan and Li [20], Eastman et al. [21], and Mintsa et al. [22]. The diameter, length, number of walls, van der Waals forces, chirality, and fabrication quality of nanotubes all influence the overall performance and properties. Carbon nanotubes (CNTs) are carbon molecules that are cylindrical in shape and consist of folded sheets of single-layer or multilayer carbon atoms (graphene). Choi et al. [16] made an analysis of the oil-based carbon nanotubes, showing that a significant enhancement in the thermal conductivity of the base fluid can be produced for dispersing of a very ordinary amount of nanotubes (~1 vol%). The aforementioned studies have been extended in many ways by Trisaksri and Wongwises [23], Wang and Mujumdar [24], Eastman et al. [25], and Kakac and Pra-muanjaroenkij [26], among others. CNTs are usually of two configurations—*single-wall* carbon nanotubes (SWCNTs) and *multiwall* carbon nanotubes (MWCNTs). CNTs have diameter that scales from ~1 to ~100 nm, and the length is of a much greater order (micrometer). Carbon nanotube has higher thermal properties with the same volume fraction compared to other nanoparticles, as noted in the study by Maré et al. [27] and Liu et al. [28]. The enhancement of convective heat transfer performance and thermal conductivity of base fluids can be achieved by CNTs successfully. Garg et al. [29] examined the impact of ultrasonication on viscous and heat transfer characteristics of MWCNTs suspended in water, identifying an enhancement of 20% in the thermal conductivity. Xue [30] developed a mathematical model for effective thermal conductivity of carbon nanotube-based composites using the Maxwell theory and considering carbon nanotube orientation distribution. Ding et al. [31] investigated CNT nanofluids over a horizontal tube and observed significant growth of the convective heat transfer, also noting a strong variation due to Reynolds number and solid volume fraction of CNTs. Sharma et al. [32] studied novel microbial fuel cell applying novel electron mediators and CNT-based electrodes, observing that almost 600% elevation in the power density (2470 mW/m^2) is obtained with CNTs compared with graphite electrodes. Kamali and Binesh [33] examined the numerical study of the convective heat transfer in the presence of constant wall heat flux condition of MWCNT-based nanofluids in a straight tube. They solved the Navier–Stokes and energy conservation equations by the finite volume method for power-law rheological CNT-based nanofluids. They conclude that the non-Newtonian behavior of CNT-based nanofluid is the reason for the change in the heat transfer coefficient created by the wall region. Khan et al. [34] examined the convective heat transfer of both SWCNT- and MWCNT-based nanofluids where the Navier slip condition exists over a flat plate. Sher Akbar et al. [35] and Khan et al. [36] studied the effects of an induced magnetic field on the peristaltic flow with SWCNTs and MWCNTs in a permeable channel over a static/moving wedge, respectively, concluding significant effects of various parameter on both CNT-based nanofluids. Convective heat transfer characteristics of secondary refrigerant-based CNT nanofluids over a tubular heat exchanger were discussed by Kumaresan et al. [37], achieving an enhancement of 160% in the convective heat transfer coefficient for the nanofluid that contains 0.45 vol % MWCNT.

The aforementioned discussions have verified the significant modification in heat transfer characteristics attainable with doping of base fluids with carbon nanotubes. However, they have been restricted to single-phase flows and have not considered melting dynamics. In recent years, significant interest in phase change materials has emerged. These produce high thermal storage density while requiring less mass and volumes of material [38–40]. When combined with nanofluids, yet further advantages may be derived. Melting heat transfer is also very important in the synthesis of engineering materials. Several studies of melting effects in thermal convection flows have been communicated. Bachok et al. [41] used Runge–Kutta–Fehlberg shooting quadrature to compute the steady two-dimensional stagnation point heat transfer to a melting stretching/shrinking sheet, noting that solutions for a shrinking sheet are nonunique. Other studies include the studies by Viswanath and Jaluria [42] (on cavity melting flows), Prescott and Incropera [43] (on alloy phase change dynamics), Jaluria [44] (on stretching sheet flows), Venkatadri et al. [45] (on electromagnetic convection in enclosures), and Gupta et al. [46] (on stagnation point micropolar convection from extending/contracting sheets). In recent years, several works on nanofluid melting convection flows have also appeared. Gupta et al. [46] analyzed the melting hydromagnetic slip convection flow in an Eyring–Powell nanofluid in a nonlinear stretching sheet. Amirsom et al. [47] computed the effects of melting and viscous heating in magneto-nanofluid bioconvection with slip effects. These studies, however, considered the Buongiorno two-component nanoscale model and did not include carbon nanotubes. Although CNT nanofluid melting dynamics studies are rare, Muhammad et al. [48] have computed the time-dependent squeezing flow of hybrid nanofluid (i.e., CNTs and CuO nanoparticles) and CNT-aqueous nanofluid with melting and viscous dissipation. They observed that the flow is accelerated with larger values of squeezing parameter, nanoparticle volume fraction for single-walled CNTs or MWCNTs, and melting parameter and nanoparticle volume fraction for copper oxide in the case of both nanofluid and hybrid nanofluid flows. The rate of heat transfer or Nusselt number is elevated with a larger estimation of squeezing parameter, nanoparticle volume fraction for copper oxide, melting parameter, and nanoparticle volume fraction for single-walled CNTs or MWCNTs, and furthermore, that entropy production rate is higher for squeezing parameter, melting parameter, and Eckert number, whereas Bejan number is reduced. CNTs nanofluid through stagnation flow with melting heat transfer has also been considered by Hayat et al. [49] for the case of an impermeable stretching sheet along with variable thickness, considering both SWCNT and MWCNT, water and kerosene oil as the base fluids. They presented homotopy solutions for the nondimensional boundary value problem and observed that temperatures are boosted with melting, and furthermore, that flow acceleration is greater with larger wall thickness for CNT–water nanofluids compared with CNT–kerosene oil nanofluids.

The main focus of the present investigation is to expand the experiment executed by Bachok et al. [41] on stagnation flow of Newtonian fluids. Both water- and kerosene-based SWCNT and MWCNT nanofluids are considered, following Khan et al. [36] with a carbon nanotube model based on the study by Xue [30] formulation. Bachok et al. [41] considered the effects of *melting heat transfer* in

boundary layer stagnation point flow of a Newtonian fluid toward a stretching/shrinking sheet. In the current study, we significantly extend that work to include convective boundary conditions and CNT nanofluids for *melting* stagnation point flow over a *stretching* sheet. Furthermore, a stability analysis is also conducted to determine upper and lower branch dual solutions at specific (critical) values of the sheet stretching parameter. These aspects all constitute the substantial novelty of the current work. It is envisaged that the present simulations are of relevance to phase change fabrication transport phenomena in carbon-based nanofluids for solar thermal energy systems [50,51]. The transformed, dimensionless boundary value problem is solved by employing the bvp4c solver in MATLAB [52].

2 Melting Carbon Nanotube Nanofluid Stagnation Flow Model

Consider the steady, two-dimensional, stagnation point flow of CNT nanofluid with phase change (melting) over a stretching sheet. The nanofluid is composed of SWCNTs and MWCNTs added to base liquids (kerosene oil or water), and the following assumptions are made:

(i) The base fluids and suspended nanoparticles (CNTs) are assumed to be in thermal equilibrium with no slip occurring.
(ii) The sheet surface is taken along the x-axis and the nanofluid is considered in the region of $y>0$.
(iii) The velocity of the external flow is $u_e(x)=ax$, where a and c are positive constants, i.e., a moving freestream is considered.
(iv) The sheet is taken to be stretched along the x-axis with a velocity $u_w(x)=cx$. The temperature of the melting surface is T_m, while the constant temperature in the freestream (edge of the boundary layer regime) is T_∞, where $T_\infty > T_m$.
(v) Viscous dissipation, thermal stratification, and heat generation/absorption effects are neglected. The coordinate system visualizes the physical model shown in Fig. 1.

The continuity, momentum, and energy equations under the usual boundary layer approximations, following Bachok et al. [41] and Khan et al. [34], may be stated as follows:

$$\frac{\partial u}{\partial x}+\frac{\partial v}{\partial y}=0 \tag{1}$$

$$u\frac{\partial u}{\partial x}+v\frac{\partial u}{\partial y}=u_e\frac{du_e}{dx}+\nu_{nf}\frac{\partial^2 u}{\partial y^2} \tag{2}$$

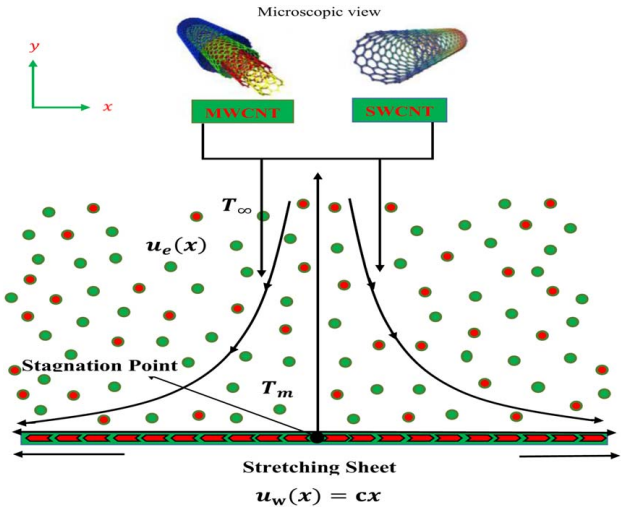

Fig. 1 Physical model CNT nanofluid stagnation flow regime

$$u\frac{\partial T}{\partial x}+v\frac{\partial T}{\partial y}=\alpha_{nf}\frac{\partial^2 T}{\partial y^2} \tag{3}$$

In the aforementioned equations, u and v are the velocity components along the x-axis and y-axis, respectively; a, $c>0$ are taken as constants; ν_{nf} is the kinematic viscosity of the nanofluid; α_{nf} is the thermal diffusivity of the nanofluid; and T is the temperature. The prescribed boundary conditions are as follows:

$$\begin{aligned} u&=u_w(x)\ \ T=T_m \quad \text{at } y=0\\ u&=u_e(x)\ \ T=T_\infty \quad \text{at } y\to\infty \end{aligned} \tag{4}$$

The melting heat transfer [45–49,53] is defined by:

$$\kappa_{nf}\left(\frac{\partial T}{\partial y}\right)_{y=0}=\rho_{nf}[\lambda+C_s(T_m-T_0)]v(x,0) \tag{5}$$

Here, κ_{nf} is the thermal conductivity of the nanofluid, λ is the latent heat of the fluid, and C_s is the heat capacity of the solid surface. In terms of the properties of base fluid and carbon nanotubes, and the solid volume fraction of CNTs in the base fluid, the effective properties of nanofluids may be expressed as follows [48,49]:

$$\mu_{nf}=\frac{\mu_f}{(1-\varphi)^{2.5}},\ \nu_{nf}=\frac{\mu_{nf}}{\rho_{nf}}$$

$$\rho_{nf}=(1-\varphi)\rho_f+\varphi\rho_{\mathrm{CNT}},\ \alpha_{nf}=\frac{\kappa_{nf}}{(\rho C_p)_{nf}} \tag{6}$$

$$(\rho C_p)_{nf}=(1-\varphi)(\rho C_p)_f+\varphi(\rho C_p)_{\mathrm{CNT}}$$

Thermal conductivity ratio is modeled using the following equation:

$$\frac{\kappa_{nf}}{\kappa_f}=\frac{(1-\varphi)+2\varphi\dfrac{\kappa_{\mathrm{CNT}}}{\kappa_{\mathrm{CNT}}-\kappa_f}ln\dfrac{\kappa_{\mathrm{CNT}}+\kappa_f}{2\kappa_f}}{(1-\varphi)+2\varphi\dfrac{\kappa_f}{\kappa_{\mathrm{CNT}}-\kappa_f}ln\dfrac{\kappa_{\mathrm{CNT}}+\kappa_f}{2\kappa_f}} \tag{7}$$

Here, μ_f denotes the viscosity of the base fluid, φ denotes the nanoparticle fraction, $(\rho C_p)_{nf}$ denotes the effective heat capacity of a nanoparticle, and ρ_{nf} denotes the density of the nanofluid. The use of the term for $\frac{\kappa_{nf}}{\kappa_f}$ is adopted from the study by Xue [30] based on the Maxwell theory, which considers that the thermal conductivity has an impact on space distribution of carbon nanotubes. We employ the following similarity transformations to nondimensionalize the conservation equations (1)–(4) following the study by Bachok et al. [41]:

$$\psi=\sqrt{(a\nu_f)}\,xf(\eta),\ \theta(\eta)=\frac{T-T_m}{T_\infty-T_m},\ \eta=\sqrt{\left(\frac{a}{\nu_f}\right)}\,y \tag{8}$$

Here, the dimensional stream function can be denoted by ψ defined via the Cauchy–Riemann equations, $u=\frac{\partial\psi}{\partial y}$ and $=-\frac{\partial\psi}{\partial x}$, for which the continuity equation (1) is satisfied automatically. By using this definition, we have:

$$u=\frac{\partial}{\partial y}\left[\sqrt{(a\nu_f)}\,xf(\eta)\right]=\sqrt{(a\nu_f)}\,x\,f'(\eta)\sqrt{\left(\frac{a}{\nu_f}\right)}=axf'(\eta) \tag{9}$$

It follows that

$$u=axf'(\eta) \tag{10}$$

Similarly:

$$v=-\frac{\partial}{\partial x}\left[\sqrt{(a\nu_f)}\,xf(\eta)\right]=-\sqrt{(a\nu_f)}\,f(\eta) \tag{11}$$

This gives:

$$v = -\sqrt{(a\nu_f)}\, f(\eta) \tag{12}$$

Finally, the transformed nonlinear coupled momentum and energy boundary layer equations emerge in ordinary differential form as follows:

$$\frac{f'''}{(1-\varphi)^{2.5}} - \left[(1-\varphi) + \varphi\frac{\rho_{\mathrm{CNT}}}{\rho_f}\right](f'^2 - f\,f'' - 1) = 0 \tag{13}$$

$$\left(\frac{\kappa_{nf}}{\kappa_f}\right)\theta'' + \mathrm{Pr}\left[(1-\varphi) + \frac{\varphi(\rho C_P)_{\mathrm{CNT}}}{(\rho C_P)_f}\right] f\,\theta' = 0 \tag{14}$$

Here, primes denote differentiation with respect to transverse coordinate, η, and $\mathrm{Pr} = \dfrac{\mu_f C_p}{\kappa_f}$ is the Prandtl number.

The transformed boundary condition become,

$$\theta(0) = 0 \quad \theta(\infty) = 1 \tag{15}$$

$$f'(0) = \varepsilon \quad f'(\infty) = 1 \tag{16}$$

The additional melting boundary condition has the form:

$$\left(\frac{\kappa_{nf}}{\kappa_f}\right) M\theta'(0) + \mathrm{Pr}\left[(1-\varphi) + \frac{\varphi\rho_{\mathrm{CNT}}}{\rho_f}\right] f(0) = 0 \tag{17}$$

where $M = \dfrac{C_p(T_\infty - T_m)}{[\lambda + C_s(T_m - T_0)]}$ is the dimensionless melting parameter and C_p is the heat capacity of the nanofluid at constant pressure. A combination of the Stefan numbers $C_f(T_\infty - T_m)/\lambda$ and $C_s(T_m - T_0)/\lambda$ is the melting parameter for the liquid and solid phases, respectively. This present study seeks to determine dual solutions for specified values of the stretching parameter, ε, and a specific range of velocity ratio parameter, i.e., $u_e(x)/u_w(x)$ for which duality exists. The stable (upper branch) solution and unstable (lower branch) solution are selected from the dual solutions. Extensive computations of the evolution of velocity, temperature, and other characteristics are also computed. The other characteristics are the *local skin friction coefficient* and *local Nusselt number* (heat transfer rate at the sheet), which are defined, respectively, as follows:

$$C_f\,\mathrm{Re}_x^{1/2} = \frac{1}{(1-\varphi)^{2.5}} f''(0) \tag{18}$$

$$\mathrm{Nu}_x\mathrm{Re}_x^{-1/2} = -\frac{\kappa_{nf}}{\kappa_f}\,\theta'(0) \tag{19}$$

3 MATLAB Numerical Solution

In the context of bvp4c function described in MATLAB [52], the fifth-order nonlinear ordinary differential equations are altered into five first-order ordinary differential equations. Based on suitable initial guesses of $f, f', f'', \theta,$ and θ', one can determine the first solution (or upper branch) and second solution (or lower branch). Equations (13) and (14) become:

$$f''' = (1-\varphi)^{2.5}\left[(1-\varphi) + \varphi\frac{\rho_{\mathrm{CNT}}}{\rho_f}\right](f'^2 - f\,f'' - 1) \tag{20}$$

$$\theta'' = -\left(\frac{\kappa_f}{\kappa_{nf}}\right)\mathrm{Pr}\left[(1-\varphi) + \frac{\varphi(\rho C_P)_{\mathrm{CNT}]}}{(\rho C_P)_f}\right] f\,\theta' \tag{21}$$

Next Eqs. (20) and (21) are transformed into first-order differential equations. We set $\eta = x$ and implement the following substitutions:

$$y_1 = f, \quad y_2 = f', \quad y_3 = f'', \quad y_4 = \theta, \quad y_5 = \theta' \tag{22}$$

The corresponding first-order differential equations are obtained as follows:

$$\frac{dy_1}{dx} = f' = y_2 \tag{23a}$$

$$\frac{dy_2}{dx} = f'' = y_3 \tag{23b}$$

$$\frac{dy_3}{dx} = f''' = (1-\varphi)^{2.5}\left[(1-\varphi) + \varphi\frac{\rho_{\mathrm{CNT}}}{\rho_f}\right](y_2^2 - y_1y_3 - 1) \tag{23c}$$

$$\frac{dy_4}{dx} = \theta' = y_5 \tag{23d}$$

$$\frac{dy_5}{dx} = \theta'' = -\left(\frac{\kappa_f}{\kappa_{nf}}\right)\mathrm{Pr}\left[(1-\varphi) + \frac{\varphi(\rho C_P)_{\mathrm{CNT}}}{(\rho C_P)_f}\right] y_1y_5 \tag{23e}$$

Next, boundary conditions (Eqs. (15)–(17)) are transformed. We set *ya* as the left boundary and *yb* as the right boundary in the numerical procedure:

$$ya(2) - \varepsilon = 0 \tag{24a}$$

$$ya(4) = 0 \tag{24b}$$

$$\left(\frac{\kappa_{nf}}{\kappa_f}\right) Mya(5) + \mathrm{Pr}\left[(1-\varphi) + \frac{\varphi\rho_{\mathrm{CNT}}}{\rho_f}\right] ya(1) = 0 \tag{24c}$$

$$yb(2) - 1 = 0 \tag{24d}$$

$$yb(4) - 1 = 0 \tag{24e}$$

4 Thermophysical Data

The heat transfer and the flow of both SWCNTs and MWCNTs in two different base fluids (water and kerosene oil) are to be explored. Thermophysical properties of two base fluids, water (i.e., $\rho = 997$ kg/m^3, $C_p = 4179$ J/kg K, $k = 0.613$ W/m K) and kerosene oil (i.e., $\rho = 783$ kg/m^3, $C_p = 2090$ J/kg K, $k = 0.145$ W/m K), as well as two CNTs, SWCNT (i.e., $\rho = 2600$ kg/m^3, $C_p = 425$ J/kg K, $k = 600$ W/m K) and MWCNT (i.e., $\rho = 1600$ kg/m^3, $C_p = 796$ J/kg K, $k = 3000$ W/m K), are taken on the data provided in Hone et al. [54] and Antar et al. [55].

The variation in the thermophysical properties of two CNT nanofluids with solid volume fraction parameter φ ranging from 0 to 0.20 with corresponding ρ, $\rho C_p(\times 10^6)$, and k of water and kerosene has taken for further computation based on the data extracted from the study by Khan et al. [34].

In the simulations, two different base fluids (water and kerosene oil) are utilized with their respective Prandtl numbers kept constant, i.e., $\mathrm{Pr} = 6.2$ for water and $\mathrm{Pr} = 21$ for kerosene. The range of the melting parameter M is 0–3, which is feasible for phase change nanomaterials [48,49]. The range of the stretching parameter $\varepsilon = \dfrac{c}{a}$ is −1.5 to 1.5. Negative values imply a shrinking sheet, and positive values imply a stretching sheet.

5 MATLAB Computation Validation, Results, and Discussion

Equations (13) and (14) with boundary conditions (Eqs. (15)–(17)) are solved numerically employing the bvp4c package in MATLAB in terms of several values of solid volume fraction (φ), Prandtl number (Pr), melting parameter (M), and stretching parameter (ε). Kierzenka and Shampine [56] introduced the excellent bvp4c function in order to facilitate the solution of nonlinear, coupled two-point

Table 1 Comparison of values of $f''(0)$ for several values of $\varepsilon = c/a$ when $\varphi = M = 0$

φ	M	ε	Wang [57]	Kimiaeifar et al. [58]	Bachok et al. [41]	Present study (first solution)	Present study (second solution)
0	0	0	1.232588	1.23258762	1.2325877	1.232591	0.850371
		0.1	1.14656	1.14656098	1.1465610	1.146563	0.753364
		0.2	1.05113	1.05112998	1.0511300	1.051132	0.646781
		0.5	0.71330	0.71329495	0.7132949	0.713296	0.274651
		1	0	0	0	0	0
		2	−1.88731	−1.88731	−1.8873066	−1.887307	−2.510919

Table 2 Error tolerance of MATLAB bvp4c solver (for several values of $\varepsilon = c/a$ when $\varphi = M = 0$ and $\varepsilon = 0$)

		First solution			Second solution		
RelTol	AbsTol	Iterations	Maximum residual	$f''(0)$	Iterations	Maximum residual	$f''(0)$
1.0×10^{0}	1.0×10^{-3}	100	2.437×10^{-1}	1.232623	110	2.413×10^{-1}	0.850371
1.0×10^{-1}	1.0×10^{-4}	145	1.130×10^{-3}	1.232534	194	4.388×10^{-2}	0.850371
1.0×10^{-2}	1.0×10^{-5}	137	3.583×10^{-3}	1.232345	202	1.409×10^{-3}	0.850371
1.0×10^{-3}	1.0×10^{-6}	147	2.716×10^{-4}	1.232564	370	4.855×10^{-4}	0.850371
1.0×10^{-4}	1.0×10^{-7}	209	8.298×10^{-5}	1.232591	456	7.877×10^{-5}	0.850371
1.0×10^{-5}	1.0×10^{-8}	189	9.119×10^{-6}	1.232591	500	3.133×10^{-6}	0.850371
1.0×10^{-6}	1.0×10^{-9}	275	9.622×10^{-7}	1.232591	610	9.847×10^{-7}	0.850371
1.0×10^{-7}	1.0×10^{-10}	510	9.977×10^{-8}	1.232591	632	9.784×10^{-8}	0.850371

boundary value problems in ordinary differential form. We consider the existence of dual solutions for specified ranges of the stretching sheet parameter. Numerical MATLAB results are first verified by comparison with simpler outcomes in the existing literature [41,57,58] for boundary layer flow without CNTs and with no melting parameter ($\varphi = M = 0$). Table 1 shows that very good compliance occurred confirming the exactness of the MATLAB solver. In this approach, we took a sufficient large value of ε at which we get convergent solution accurate up to seven digits, which is shown in Table 2.

Values of reduced skin friction $f''(0)$ for $\varphi \neq 0$ are also documented in Table 3. $\varphi = 0$ corresponds to a regular viscous fluid. The scale of nanoparticle volume fraction considered is from 0 to 0.2 ($0 < \varphi < 0.2$).

Figures 2 and 3 are plotted to study the accuracy of the MATLAB bvp4c solver by comparing the velocity profile $f'(\eta)$ and temperature profile $\theta(\eta)$ for $\varepsilon = 0.2$, $\mathrm{Pr} = 6.2$, $\varphi = 0$ again with those obtained in the literature, i.e., the study by Bachok et al. [41]. Once again very good correlation is achieved testifying to the high accuracy of the MATLAB bvp4c solver, at all values of melting parameter, M. Invariably, both velocity and temperatures are suppressed with a greater melting effect.

5.1 Skin Friction Analysis. Figures 4–7 illustrate the impact of melting parameter (M) on the variation of dimensionless skin friction $f''(0)$ for SWCNTs and MWCNTs of water- and kerosene oil-based fluids, respectively. It can be seen that a dual solution exists for $\varepsilon > \varepsilon_c$ for both water- and kerosene-based SWCNT and MWCNT. However, no solution exists for $\varepsilon < \varepsilon_c$. Physically this implies that there is boundary layer separation and a breakdown of laminar boundary layer approximations, where ε_c is the critical value of ε. The variation of ε_c has been shown in Table 4, for which a favorable agreement has been observed with those reported by Bachok et al. [41] for the case of M, when $\varphi = 0$.

Figures 4 and 5 depict the variations of the skin friction coefficient $f''(0)$ for stretching parameter, ε, with several values of melting parameter M for both water-based SWCNT and MWCNT nanofluids. It is apparent that for these values of melting parameter, two critical values $\varepsilon_c = -1.252$ and $\varepsilon_c = -1.253$ are identified,

Table 3 Comparison of values of $f''(0)$ of water- and kerosene oil-based SWCNT and MWCNT nanofluids

	Pr	φ	M	ε	Bachok et al.'s [41] first solution	Bachok et al.'s [41] second solution	Present study (first solution)	Present study (second solution)
	1	0	0	0	1.2325877		1.232591	0.850371
				0.1	1.1465610		1.146563	0.753364
				0.2	1.05113		1.051132	0.646781
Water (SWCNT)	6.2	0.1	0	0			1.164116	0.737720
				0.1			1.082868	0.646489
				0.2			0.992739	0.546111
Water (MWCNT)	6.2	0.1	0	0			1.112686	0.645333
				0.1			1.035028	0.558970
				0.2			0.948880	0.463724
Kerosene (SWCNT)	21	0.1	0	0			1.199323	0.796949
				0.1			1.115618	0.702668
				0.2			1.022763	0.599027
Kerosene (MWCNT)	21	0.1	0	0			1.135463	0.687182
				0.1			1.056215	0.598593
				0.2			0.968303	0.501013

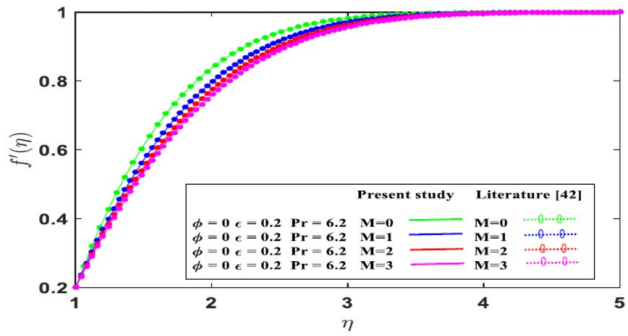

Fig. 2 Comparison of dimensionless velocity $f'(\eta)$

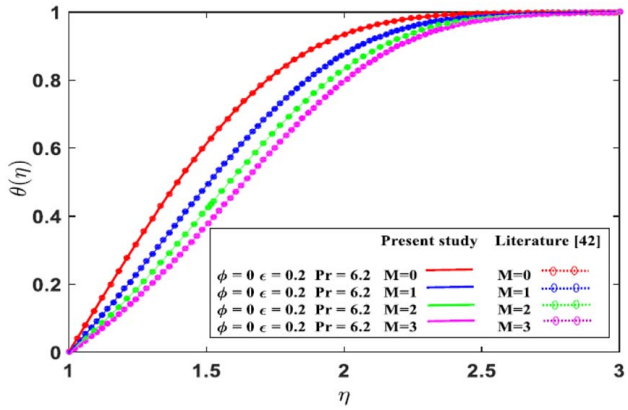

Fig. 3 Comparison of dimensionless temperature $\theta(\eta)$

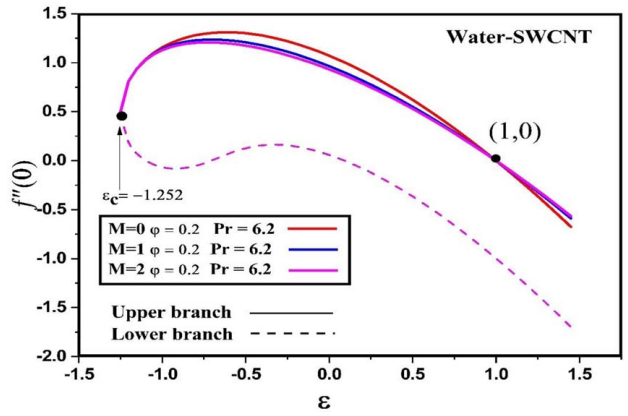

Fig. 4 Effects of melting parameter (M) on dimensionless skin friction coefficient $f''(0)$ of water-based SWCNT nanofluid as a function of stretching parameter (ε) when Pr = 6.2 and $\varphi = 0.2$

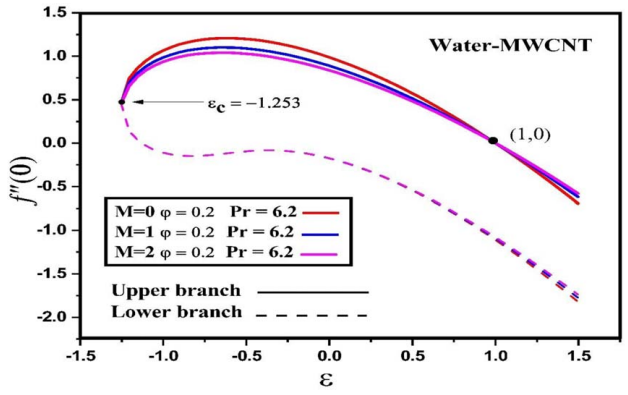

Fig. 5 Effects of melting parameter (M) on dimensionless skin friction coefficient $f''(0)$ of water-based MWCNT nanofluid as a function of stretching parameter (ε) when Pr = 6.2 and $\varphi = 0.2$

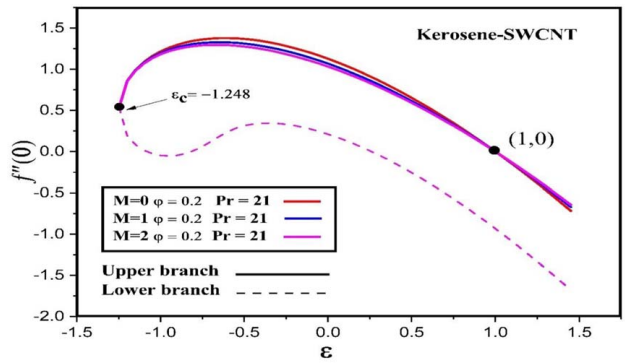

Fig. 6 Effects of melting parameter (M) on dimensionless skin friction coefficient $f''(0)$ of kerosene oil-based SWCNT nanofluid as a function of stretching parameter (ε) when Pr = 21 and $\varphi = 0.2$

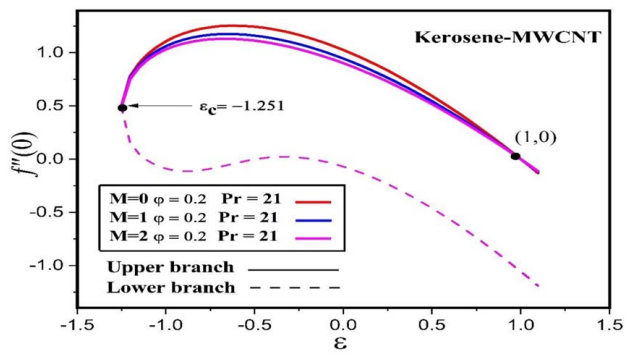

Fig. 7 Effects of melting parameter (M) on dimensionless skin friction coefficient $f''(0)$ of kerosene oil-based MWCNT nanofluid as a function of stretching parameter (ε) when Pr = 21 and $\varphi = 0.2$

respectively, for SWCNT and MWCNT water-based nanofluid. Evidently a dual solution exists for $\varepsilon > \varepsilon_c = -1.252$ and no solution exists for $\varepsilon < \varepsilon_c = -1.252$ for SWCNT nanofluid. Additionally, a dual solution exists for $\varepsilon > \varepsilon_c = -1.253$ and no solution exists for $\varepsilon < \varepsilon_c = -1.253$ for MWCNT nanofluid.

Larger values of melting parameter modify skin friction coefficient. We can conclude that the values of skin friction decrease with the rising melting parameter for both water-based SWCNT and MWCNT nanofluids, i.e., greater phase change induced strong deceleration in the boundary layer flow and increases momentum boundary layer thickness. Figures 6 and 7 depict the variations of the skin friction coefficient $f''(0)$ for stretching parameter, ε, with selected values of melting parameter M for both kerosene-based SWCNT and MWCNT nanofluids. Again, two critical values of stretching rate parameter arise, i.e., $\varepsilon_c = -1.248$ and $\varepsilon_c = -1.251$, respectively, for SWCNT and MWCNT kerosene-based nanofluid. Close inspection of the graphs reveals that a dual solution exists for $\varepsilon > \varepsilon_c = -1.248$ and no solution exists for $\varepsilon < \varepsilon_c = -1.248$ for SWCNT nanofluid. Additionally, a dual solution exists for $\varepsilon > \varepsilon_c = -1.251$ and no solution exists for $\varepsilon < \varepsilon_c = -1.251$ for MWCNT nanofluid. Larger values of melting parameter strongly suppress

Table 4 Values of ε_c for various values of melting parameter M, when Pr = 1

M	Bachok et al. [41]	Present work
0	−1.24657	−1.2461
1	−1.23617	−1.23250
2	−1.22931	−1.22520
3	−1.22414	−1.22403

the skin friction coefficient. For both kerosene-based SWCNTs and MWCNTs, the values of skin friction decrease with the increasing melting parameter, i.e., more intense phase change. However, for both water- and kerosene-based nanofluids, the skin friction of SWCNTs is observed to be greater compared to MWCNTs. For both types of CNTs, skin friction decreases. It is noted that skin friction values are higher for kerosene oil-based CNT nanofluids than that of water-based CNT nanofluids.

Figures 8–11 illustrate the nature of nanoparticle volume fraction φ of the change of dimensionless skin friction $f''(0)$ for both SWCNT and MWCNT for water as well as kerosene oil-based fluids, respectively. It can be seen that a dual solution exists for $\varepsilon > \varepsilon_c$ for both water- and kerosene-based SWCNT and MWCNT. However, no solution exists for $\varepsilon < \varepsilon_c$. Physically this implies that there is boundary layer separation and a breakdown of laminar boundary layer approximations, where ε_c is the critical value of ε (boundary layer approximations and boundary layer separation are not physically attainable), where ε_c is the critical value of ε. The variation of ε_c has again been documented in Table 4, which as noted earlier, demonstrates very good correlation with the solutions of Bachok et al. [41] in terms of M, when $\varphi = 0$.

Figures 8 and 9 depict the variations of the skin friction $f''(0)$ of stretching parameter ε for selected values of φ for both water-based SWCNT and MWCNT nanofluids. It can be seen that two critical values $\varepsilon_c = -1.252$ and $\varepsilon_c = -1.253$ are identified, respectively, for SWCNT and MWCNT water-based nanofluid. A dual solution exists for $\varepsilon > \varepsilon_c = -1.252$ and no solution exists for $\varepsilon < \varepsilon_c = -1.252$ for SWCNT nanofluid. In addition, a dual solution exists for $\varepsilon > \varepsilon_c = -1.253$ and no solution exists for $\varepsilon < \varepsilon_c = -1.253$ for MWCNT nanofluid. Larger values of nanoparticle volume fraction considerably boost skin friction. We can conclude that skin friction values increase (i.e., flow acceleration is induced) with the growing nanoparticle volume fraction, for both water-based SWCNT and MWCNT nanofluids.

Figures 10 and 11 depict the variations of the skin friction coefficient $f''(0)$ with ε for several values of φ for both kerosene-based SWCNT and MWCNT nanofluids. At all considered values of φ, we have two critical values $\varepsilon_c = -1.248$ and $\varepsilon_c = -1.251$, respectively, for SWCNT and MWCNT nanofluids. Evidently a dual solution exists for $\varepsilon > \varepsilon_c = -1.248$ and no solution exists for $\varepsilon < \varepsilon_c = -1.248$ for SWCNT nanofluid. Additionally, a dual solution exists for $\varepsilon > \varepsilon_c = -1.251$ and no solution exists for $\varepsilon < \varepsilon_c = -1.251$ for MWCNT nanofluid. Skin friction coefficient is again accentuated for nanoparticle volume fraction with larger values. Overall, for both kerosene-based SWCNT and MWCNT, values

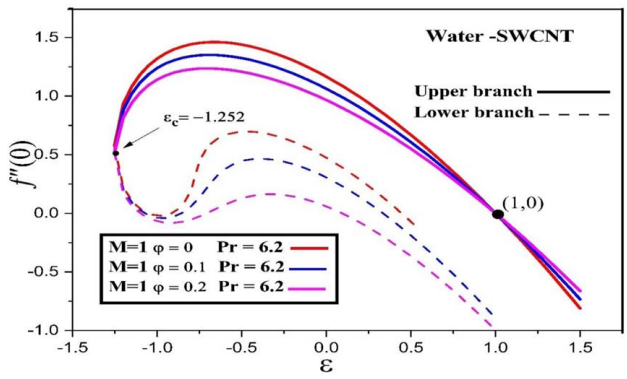

Fig. 8 Effects of nanoparticle volume fraction (φ) on dimensionless skin friction coefficient $f''(0)$ of water-based SWCNT as a function of stretching parameter (ε) when Pr = 6.2 and $M = 1$

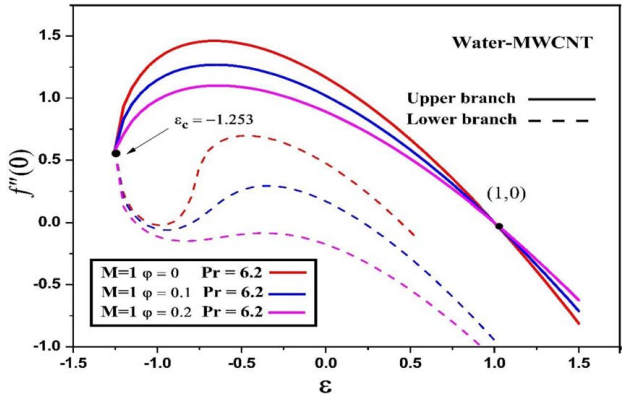

Fig. 9 Effects of nanoparticle volume fraction (φ) on dimensionless skin friction coefficient $f''(0)$ of water-based MWCNT as a function of stretching parameter (ε) when Pr = 6.2 and $M = 1$

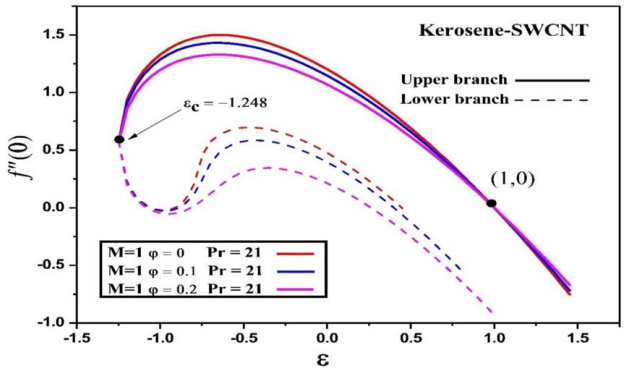

Fig. 10 Effects of nanoparticle volume fraction (φ) on dimensionless skin friction coefficient $f''(0)$ of kerosene-based SWCNT nanofluid as function of stretching parameter (ε) for Pr = 21 and $M = 1$

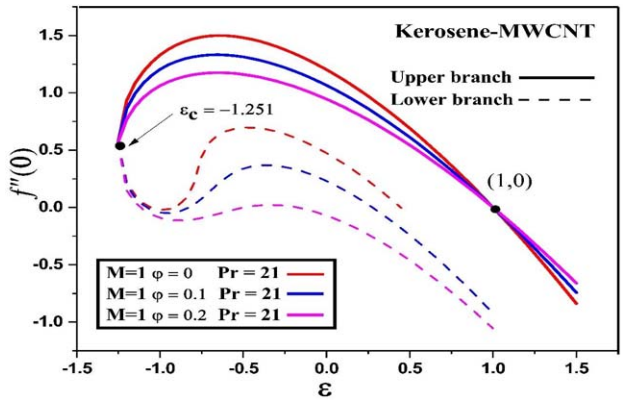

Fig. 11 Effects of nanoparticle volume fraction (φ) on dimensionless skin friction coefficient $f''(0)$ of kerosene-based MWCNT nanofluid as function of stretching parameter (ε) for Pr = 21 and $M = 1$

of skin friction are elevated with growing nanoparticle volume fraction, indicating that increased nanotube doping results in strong acceleration in the boundary layer flow. However, for both water- and kerosene-based fluids, higher skin friction is obtained for SWCNTs compared to MWCNTs. For both types of CNTs, skin friction decreases. It is also explored that greater skin friction values are found for kerosene-based nanotubes comparing with water-based nanotubes.

5.2 Heat Transfer Analysis. Figures 12–15 illustrate the impact of melting parameter M on the variation of dimensionless heat transfer $-\theta'(0)$, i.e., Nusselt number, SWCNTs, and MWCNTs of water- and kerosene-based nanofluids, respectively. It can be seen that a dual solution exists for $\varepsilon > \varepsilon_c$ for both water- and kerosene-based SWCNT and MWCNT. However, no solution exists for $\varepsilon < \varepsilon_c$. Physically this implies that there is boundary layer separation and a breakdown of laminar boundary layer approximations, where ε_c is the critical value of ε and is documented in Table 4, concurring with values computed by Bachok et al. [41] in terms of M, with $\varphi = 0$.

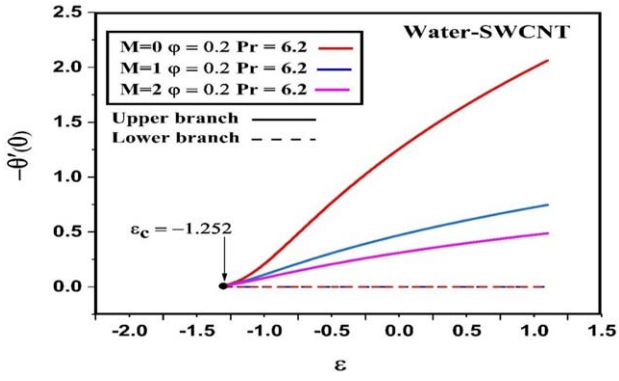

Fig. 12 Effects of melting parameter (M) on dimensionless heat transfer $-\theta'(0)$ of water-based SWCNT nanofluid as a function of stretching parameter (ε) when Pr = 6.2 and $\varphi = 0.2$

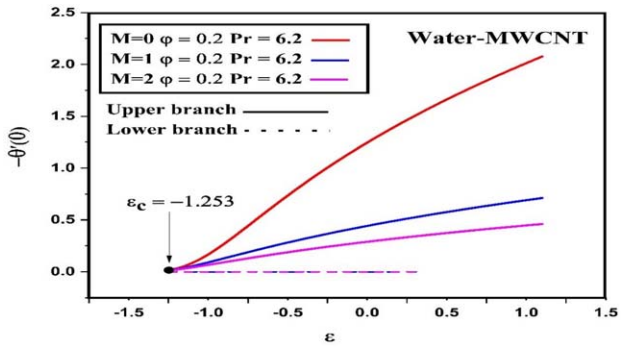

Fig. 13 Effects of melting parameter (M) on dimensionless heat transfer $-\theta'(0)$ of water-based MWCNT nanofluid as a function of stretching parameter (ε) when Pr = 6.2 and $\varphi = 0.2$

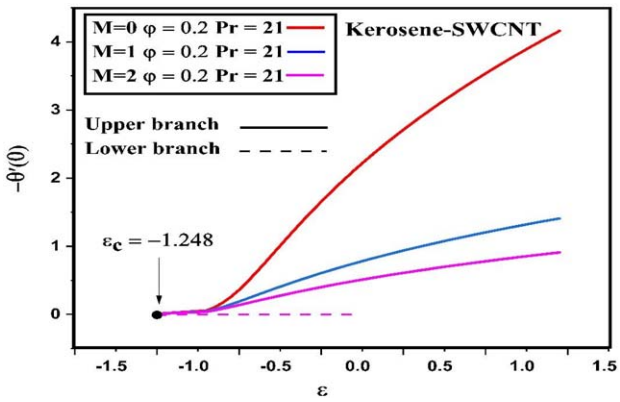

Fig. 14 Effects of melting parameter (M) on dimensionless heat transfer $-\theta'(0)$ of kerosene-based SWCNT nanofluid as a function of stretching parameter (ε) when Pr = 21 and $\varphi = 0.2$

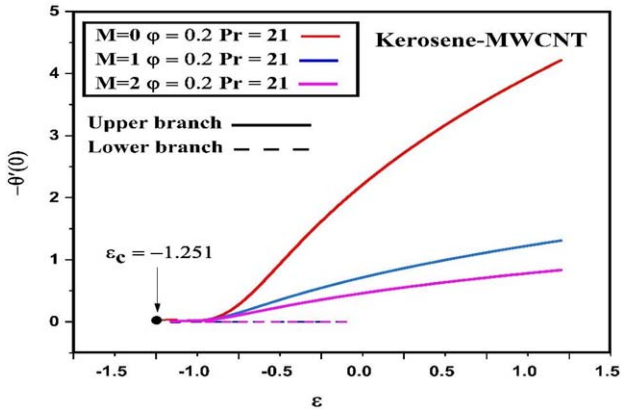

Fig. 15 Effects of melting parameter (M) on dimensionless heat transfer $-\theta'(0)$ of kerosene-based MWCNT nanofluid as a function of stretching parameter (ε) when Pr = 21 and $\varphi = 0.2$

Figures 12 and 13 indicate for the values of melting parameter examined, we have two critical values $\varepsilon_c = -1.252$ and $\varepsilon_c = -1.253$, respectively, for SWCNT and MWCNT water-based nanofluid. It can be seen that a dual solution exists for $\varepsilon > \varepsilon_c = -1.252$ and no solutions exists for $\varepsilon < \varepsilon_c = -1.252$ for the SWCNT case and that a dual solution exists for $\varepsilon > \varepsilon_c = -1.253$ and no solutions exist for $\varepsilon < \varepsilon_c = -1.253$ for the MWCNT case. Larger values of melting parameter *enhance* the dimensionless heat transfer, i.e., intensified melting increase the heat, which is transferred to the wall *from* the boundary layer. This indicates that temperatures are suppressed within the boundary layer, which is associated with phase change [47,48,53]. A boost in momentum with higher melting effect is obtained, which is increased with respect to the heat diffusion rate. Thermal boundary layer thickness is therefore reduced. Melting [48] also induces better distribution of nanotubes in the nanomaterials. Generally, for both water-based SWCNT and MWCNT nanofluids, the dimensionless heat transfer values increase with the increasing melting parameter, and thermal boundary layer thickness is depleted in both cases. Figures 14 and 15 (kerosene-based SWCNT and MWCNT nanofluids) show that there are two critical values of stretching parameter, i.e., $\varepsilon_c = -1.248$ and $\varepsilon_c = -1.251$, respectively, for SWCNT and MWCNT kerosene-based fluid. It can be seen that a dual solution exists for $\varepsilon > \varepsilon_c = -1.248$ and no solutions exist for $\varepsilon < \varepsilon_c = -1.248$ for the SWCNT nanofluid and that a dual solution exists for $\varepsilon > \varepsilon_c = -1.251$ and no solutions exist for $\varepsilon < \varepsilon_c = -1.251$ for the MWCNT nanofluid. Larger values of melting parameter again *elevate* the dimensionless heat transfer, i.e., accentuate Nusselt number at the wall. For both kerosene-based SWCNT and MWCNT nanofluids, dimensionless heat transfer values are enhanced with increasing melting.

In addition, for both water- and kerosene-based nanofluids, the dimensionless heat transfer achieved with MWCNTs is markedly higher than that generated with SWCNTs. For both types of CNTs, significant transfer of thermal energy to the wall (sheet) is induced with phase change. Also, Nusselt numbers, i.e., greater dimensionless heat transfer rates, are attained for water-based nanotubes compared to kerosene-based nanotubes.

Figures 16–19 depict the impact of nanoparticle volume fraction φ on the change of dimensionless heat transfer $-\theta'(0)$ for single-

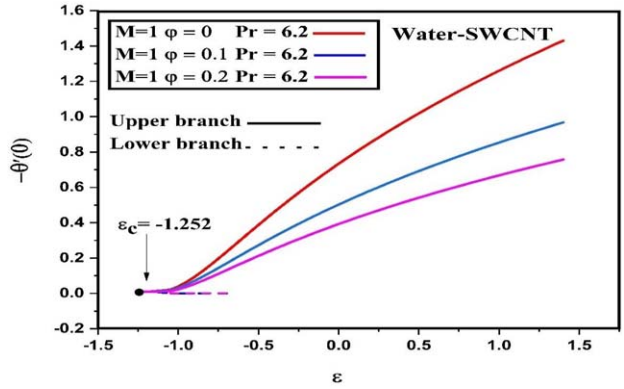

Fig. 16 Effects of nanoparticle volume fraction φ on dimensionless heat transfer $-\theta'(0)$ of water-based SWCNT nanofluid as a function of stretching parameter (ε) when Pr = 6.2 and $M = 1$

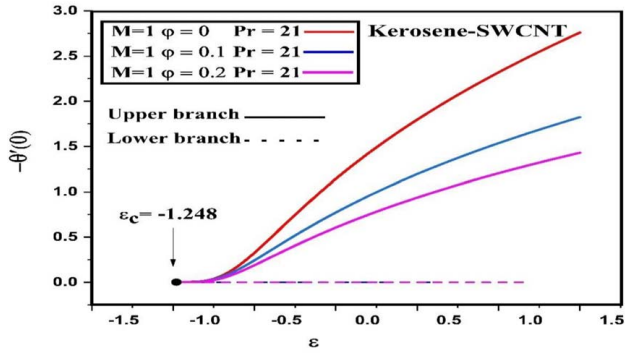

Fig. 18 Effects of nanoparticle volume fraction φ on dimensionless heat transfer $-\theta'(0)$ of kerosene-based SWCNT nanofluid as a function of stretching parameter (ε) when Pr = 6.2 and $M = 1$

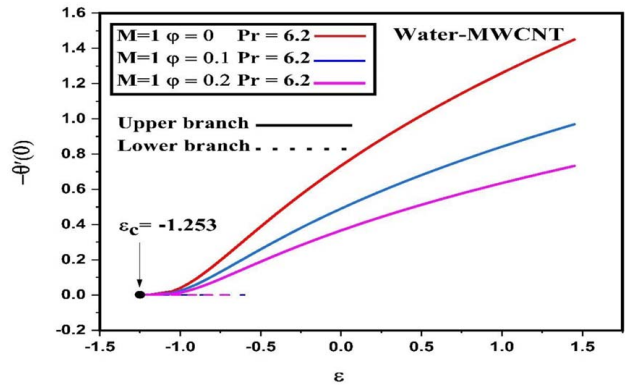

Fig. 17 Effects of nanoparticle volume fraction φ on dimensionless heat transfer $-\theta'(0)$ of water-based MWCNT nanofluid as a function of stretching parameter (ε) when Pr = 6.2 and $M = 1$

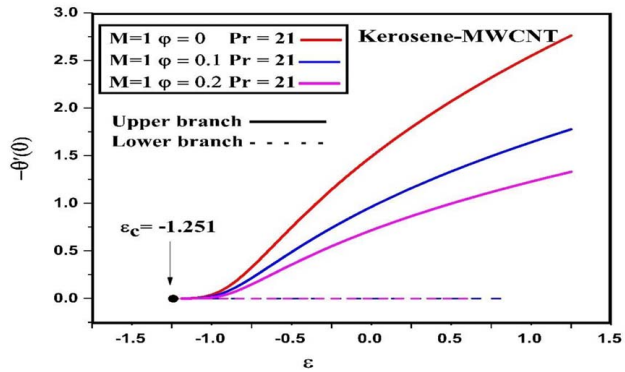

Fig. 19 Effects of nanoparticle volume fraction φ on dimensionless heat transfer $-\theta'(0)$ of kerosene-based MWCNT as a function of stretching parameter (ε) when Pr = 6.2 and $M = 1$

wall and MWCNTs of water- and kerosene oil-based fluids, respectively. Inspection of the plots shows that a dual solution exists for $\varepsilon > \varepsilon_c$ for both water- and kerosene-based SWCNT and MWCNT. However, no solution exists for $\varepsilon < \varepsilon_c$. Physically this implies that there is boundary layer separation and a breakdown of laminar boundary layer approximations, where ε_c is the critical value of ε. Figures 16 and 17 show that for all values of nanoparticle volume fraction φ, we have two critical values of the stretching parameter, $\varepsilon_c = -1.252$ and $\varepsilon_c = -1.253$, respectively, for SWCNT and MWCNT water-based nanofluid. Apparently, it can be seen that a dual solution exists for $\varepsilon > \varepsilon_c = -1.252$ and no solutions exist for $\varepsilon < \varepsilon_c = -1.252$ for the SWCNT case and that a dual solution exists for $\varepsilon > \varepsilon_c = -1.253$ and no solutions exist for $\varepsilon < \varepsilon_c = -1.253$ for the MWCNT case. Larger values of nanoparticle volume fraction φ are observed to suppress dimensionless heat transfer, i.e., Nusselt number magnitudes. Since thermal conductivity is elevated with greater doping of nanotubes, temperatures within the boundary layer will be boosted. Greater heat quantities will be convected away from the sheet into the nanofluid, resulting in a depression in heat transfer to the wall. This manifests in a plummet in Nusselt numbers. For both water-based SWCNT and MWCNT nanofluids, dimensionless heat transfer values are clearly decreased with increasing nanoparticle volume fraction, φ. In Figures 18 and 19 (kerosene-based SWCNT and MWCNT nanofluids), for the studied range of nanoparticle volume fraction φ, we have two critical values $\varepsilon_c = -1.248$ and $\varepsilon_c = -1.251$, respectively, for SWCNT and MWCNT kerosene-based nanofluids. It can be seen that a dual solution exists for $\varepsilon > \varepsilon_c = -1.248$ and no solutions exist for $\varepsilon < \varepsilon_c = -1.248$ for the SWCNT case and that a dual solution exists for $\varepsilon > \varepsilon_c = -1.251$ and no solutions exist for $\varepsilon < \varepsilon_c = -1.251$ for the MWCNT case. Increments in nanoparticle volume fraction φ are observed to diminish dimensionless heat transfer magnitudes. In terms of both kerosene-based SWCNT and MWCNT nanofluids, dimensionless heat transfer values are strongly depleted with the increasing nanoparticle volume fraction, φ. It is also noteworthy that for both water- and kerosene-based fluids, the dimensionless heat transfer of MWCNTs is significantly in excess of those computed for SWCNTs. For both types of CNTs, dimensionless heat transfer decreases with greater volume fraction, which again is due to the elevation in temperatures inside the nanofluid with higher nanotube doping, which manifests in a reduction in heat transferred away from the boundary layer. Greater dimensionless heat transfer values are attained for water-based nanotubes comparing with kerosene-based nanotubes, and this is also connected to the significantly higher thermal diffusivity of water relative to kerosene. Prandtl number for water base fluid is less than a third for kerosene-based fluid, which implies that heat is diffused much faster in the former, leading to greater temperatures in the nanofluid and lower Nusselt numbers for water-CNT nanofluid.

Table 5 shows the changes in skin friction values for volume fraction and melting parameter. It is observed that skin friction values decrease with the increasing melting parameter and increase with greater volume fraction for both *water-based* SWCNT and MWCNT nanofluids. Flow acceleration is induced in the boundary layer with greater doping of nanotubes, whereas retardation is produced with intensification in melting. Table 6 indicates that in terms of both types of CNTs in kerosene oil-based nanotubes, again skin friction coefficient increases with higher volume fraction. In the

Table 5 Variation of local Nusselt number and local skin friction with φ for different values of melting parameter M with water-based CNT nanofluids

		$\mathrm{Re}_x^{1/2}C_f$			$\mathrm{Re}_x^{-1/2}\mathrm{Nu}_x$		
Water based	φ	$M=0$	$M=1$	$M=2$	$M=0$	$M=1$	$M=2$
SWCNT	0	1.051130	0.990024	0.959064	−1.326094	−0.854376	−0.651267
	0.12	1.346983	1.217231	1.172737	−4.212007	−1.841450	−1.254022
	0.2	1.597123	1.427963	1.376651	−6.416674	−2.411400	−1.593485
MWCNT	0	1.051130	0.990027	0.959067	−1.326094	−0.854376	−0.651267
	0.12	1.2772433	1.161197	1.100963	−3.913163	−1.673975	−1.134786
	0.2	1.471004	1.322711	1.243678	−5.875801	−2.096335	−1.372974

Table 6 Variation of local Nusselt number and local skin friction with φ for different values of melting parameter M of kerosene-based CNTs

		$\mathrm{Re}_x^{1/2}C_f$			$\mathrm{Re}_x^{-1/2}\mathrm{Nu}_x$		
Kerosene based	φ	$M=0$	$M=1$	$M=2$	$M=0$	$M=1$	$M=2$
SWCNT	0	1.051132	1.020721	1.004954	−2.280127	−1.473325	−1.124956
	0.12	1.394438	1.325253	1.286311	−8.307463	−3.480093	−2.350815
	0.2	1.681065	1.587819	1.532828	−13.10054	−4.638421	−3.036485
MWCNT	0	1.051132	1.020721	1.004954	−2.280127	−1.473325	−1.124956
	0.12	1.308200	1.217342	1.169415	−7.780925	−3.125582	−2.093697
	0.2	1.527443	1.443372	1.397061	−12.17206	−3.964854	−2.561101

nonappearance of CNTs, skin friction decreases with increasing melting parameter M. In both types of CNTs, skin friction increases. It can be noted that skin friction values are higher for kerosene-based CNTs than that of water-based CNTs. Tables 5 and 6 also document the Nusselt number, i.e., wall heat transfer rate, which is clearly decreased with increasing volume fraction φ (since temperatures in the nanofluid are elevated) and increased with greater melting parameter M (since temperatures in the nanofluid are suppressed with greater phase change). A similar phenomenon occurred for both types of CNTs and both base fluids (water/kerosene oil). Nusselt number also quantifies the ratio of convection to conduction heat transfer. Greater melting therefore boosts the convection to the wall, whereas increasing volume fraction has the opposite effect.

5.3 Velocity and Temperature Fields. Figures 20–25 depict the evolution in velocity (f') and temperature (θ) distributions with various thermophysical parameters. Figures 20 and 21 illustrate the numerical solutions and dual solution obtained as well as profiles for which boundary conditions are satisfied and converge asymptotically. The figures can represent the dual solutions clearly. The existence of dual nature of the solutions can be supported by these velocity and temperature profiles. It can be seen that a dual solution exists for $\varepsilon > \varepsilon_c$ for both water- and kerosene-based SWCNT and MWCNT. However, no solution exists for $\varepsilon < \varepsilon_c$.

The variation of ε_c has been shown earlier in Table 4. It is also clearly noted that the first solution (higher magnitude) is associated with a thinner boundary layer thickness when it is compared to the second solution (lower magnitude).

We study the cases of $M=0$ (no melting), 1, 2, 3(strong melting) for SWCNTs and MWCNTs water-based fluid. Figure 20 shows that the values of the dual velocity $f'(\eta)$ reduce with the increasing M in terms of the first solution and the dual velocity reduces with the increasing M in the second solution for both SWCNT and MWCNT cases. Water-based SWCNT achieves the *highest* dual velocity, whereas the water-based MWCNT achieves the lowest

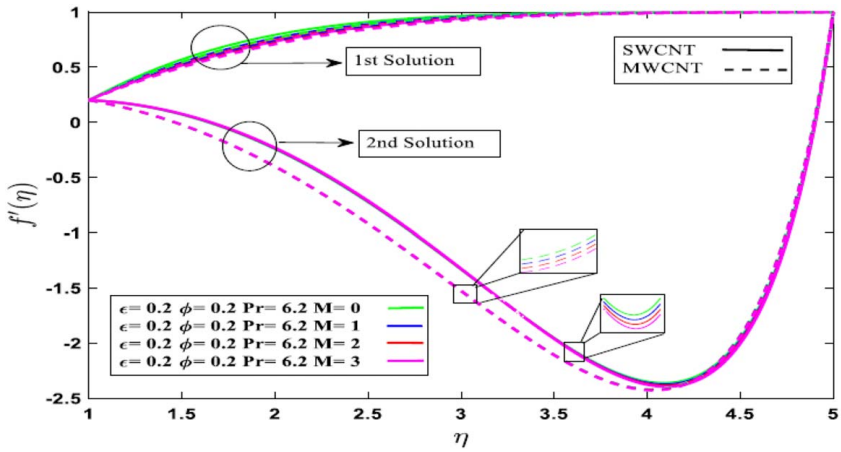

Fig. 20 Effect of various melting parameter (M) on velocity profile, $f'(\eta)$ water-based CNT nanofluids

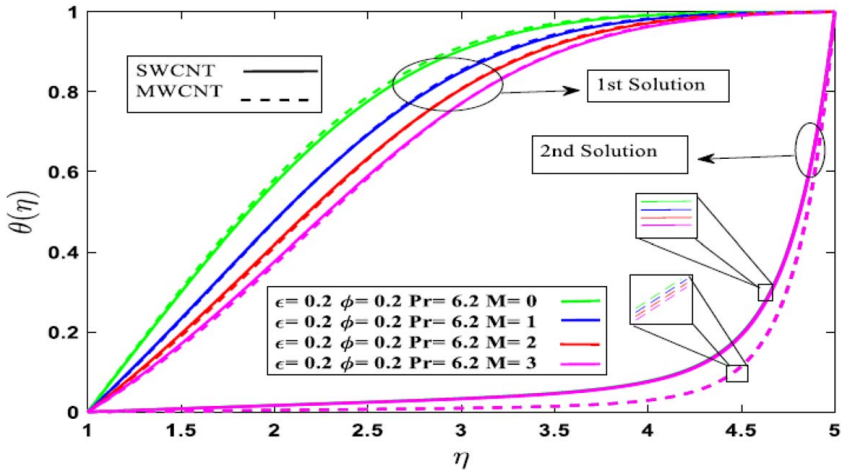

Fig. 21 Effect of various melting parameter (M) on temperature profile, $\theta(\eta)$ of water-based CNT nanofluids

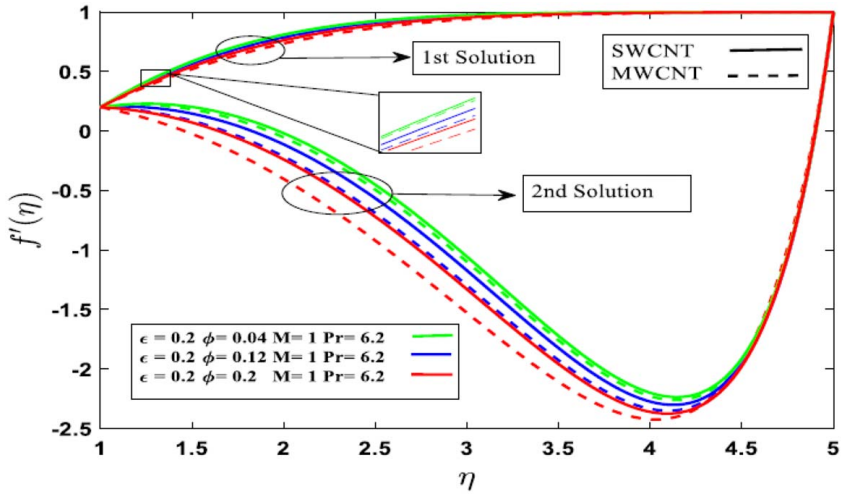

Fig. 22 Effect of nanoparticle volume fraction (φ) on velocity, $f'(\eta)$ of water-based CNT nanofluids

dual velocity. Figure 21 reveals that temperature $\theta(\eta)$ decreases with an increase of M, i.e., higher melting parameter M of both SWCNT and MWCNT nanofluids is attained for increasing thermal boundary layer thickness. As elaborated earlier, with higher melting parameter, there is an upsurge in heat transfers from the heated fluid toward the melting surface, which acts as a thermal sink. This reduces temperature magnitudes. A similar behavior has been computed by many other researchers including Jaluria [44], Gupta et al. [46], Reddy et al. [53], and Muhammad et al. [48]. In addition, the temperature magnitudes for the MWCNTs are larger than that of SWCNTs for water-based nanofluid. It is confirmed from the results that the melting phenomenon can be acted as a *thermal sink boundary condition* at the sheet surface. Consequently, more intense melting (increasing M) tends to *reduce* thermal boundary layer thickness.

Figures 22 and 23 illustrate the influence of solid volume fraction of both SWCNTs and MWCNTs of water-based fluid on velocity, $f'(\eta)$ and temperature $\theta(\eta)$. Again, asymptotically smooth distributions are computed, indicating that a sufficiently large infinity boundary condition is prescribed in the MATLAB computations. The *dual solutions* are clearly identified. It can be seen that a dual solution is identified for $\varepsilon > \varepsilon_c$, and no solutions are identified for $\varepsilon < \varepsilon_c$. It is also clearly found that the first solution (upper branch) that is of greater magnitude corresponds to a thinner momentum boundary layer thickness when it is compared to the second solution (lower branch). Here, we change the solid volume fraction (φ) and keep the other parameters fixed. Fluid velocity (Fig. 22) is generally decreased with growing φ for the first solution, and the dual velocity increases with decreasing φ for the second solution in the case of SWCNT and MWCNT. Water-based SWCNT attains the highest dual velocity, whereas the water-based MWCNT achieves the lowest dual velocity. Figure 23 shows that temperature decreases with an increase of φ *for the first solution*, whereas it increases with the increasing φ for the second solution for both SWCNT and MWCNT cases. The reason is the increase in the thermal conductivity of CNTs with the solid volume fraction. In addition, temperature values for the case of MWCNTs are larger than that of SWCNTs for the water base fluid.

Figures 24 and 25 illustrate the numerical solutions and dual solution for both CNTs of kerosene-based fluid for velocity $f'(\eta)$ and temperature $\theta(\eta)$ with several values of melting parameter, M. Again in Fig. 24, the first velocity solution is higher and hydrodynamic boundary layer thickness is thinner compared with the lower second solution. The value of the dual velocity decreases with the increasing M for the first solution, whereas no tangible modification is induced in the second solution, for both SWCNT and MWCNT cases. Kerosene-based SWCNT produces the highest dual velocity,

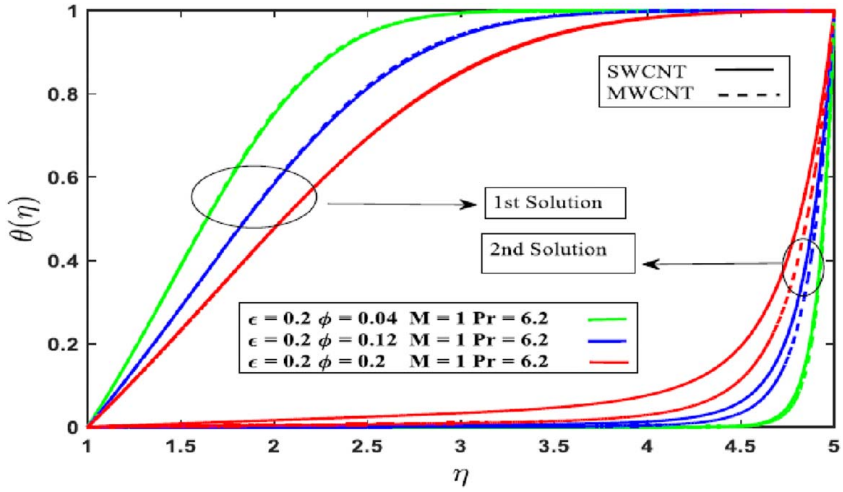

Fig. 23 Effect of nanoparticle volume fraction (φ) on temperature, $\theta(\eta)$ of water-based CNT nanofluids

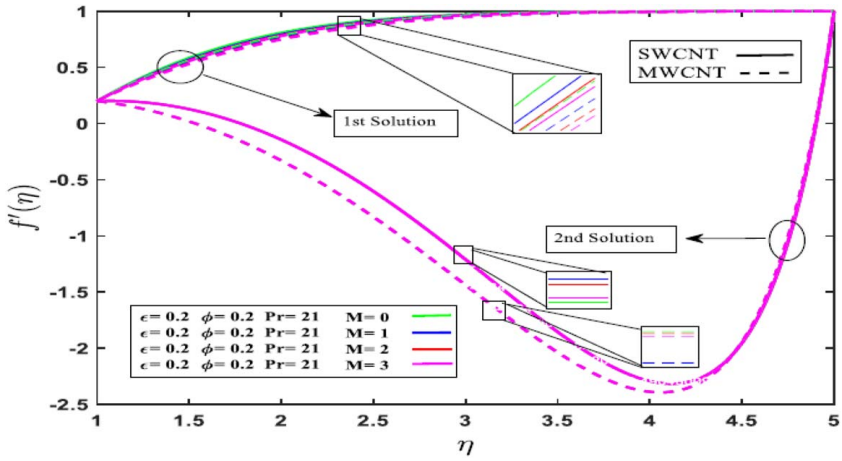

Fig. 24 Effect of various melting parameter (M) on velocity profile, $f'(\eta)$ of water-based CNT nanofluids

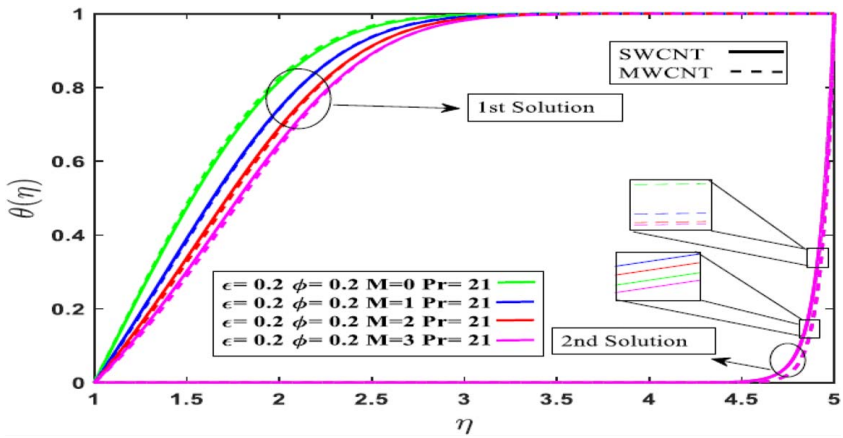

Fig. 25 Effect of various melting parameter (M) on temperature profile, $\theta(\eta)$ of Kerosene oil-based CNTs

whereas the kerosene-based MWCNT achieves the lowest dual velocity. Figure 25 shows that with an increase in M, temperature markedly decreases, and thermal boundary layer thickness is also therefore dimensionless with greater melting for both CNTs. In addition higher temperature magnitudes are produced in the case of MWCNTs compared with SWCNTs for kerosene-based fluid.

6 Concluding Remarks

In the present work, steady two-dimensional stagnation point melting convection flow of CNT nanofluids from a stretching sheet (with water and kerosene oil as base fluids) under the convective boundary condition has been analyzed. Both SWCNTs and MWCNTs have been studied. The transformed governing boundary layer equations were resolved by utilizing the robust bvp4c function in MATLAB. Results indicate that dual solutions exist. After the separation by a critical point, these solutions are called as upper branch and lower branch. The upper branch denotes a stable solution as well as the lower branch denotes an unstable solution. To validate the MATLAB computations, the numerical results obtained have been compared with the previously reported cases available from the literature, and very good correlation has been demonstrated. Effects of melting parameter, Prandtl number, nanoparticle volume fraction parameter and stretching parameter on local skin friction coefficient, local Nusselt number, velocity, and temperature distributions have been examined. The following conclusions may be drawn:

(1) The skin friction coefficient C_{fx} increases with an increase in CNT volume fraction parameter φ, whereas the Nusselt number Nu_x decreases.
(2) The skin friction C_{fx} reduces with an enhancement in melting parameter M, whereas the Nusselt number Nu_x increases.
(3) Velocity and temperature profiles decreases for higher values of melting parameter M.
(4) The impact of melting parameter M over velocity and temperature distributions has more prominence in the case of SWCNTs when it is compared with MWCNTs for water- and kerosene oil-based fluids.
(5) Velocity decreases for greater values of nanoparticle volume fraction φ, where temperature increases for the second solution computed.
(6) The influence of nanoparticle volume fraction φ on velocity and temperature is more substantial in the case of SWCNTs in comparing with MWCNTs for water- and kerosene oil-based fluids.
(7) Single-wall CNTs has more efficiency than MWCNTs and produce superior skin friction and heat transfer rate.
(8) Between kerosene-based CNTs and water-based CNTs, kerosene-based CNTs exhibit larger skin friction and heat transfer rates.
(9) With an increment in stretching parameter, the computed range of solutions is widely expanded.
(10) Critical values of skin friction and heat transfer rate are computable above which dual solutions are simulated.
(11) The first (upper branch) solution turns to a stable solution and physically relevant, while the second (lower branch) solution turns to an unstable solution.

The current investigation has been confined to plane stagnation flow of CNT nanofluids. Future simulations will consider oblique (nonorthogonal) stagnation flows [59], which are also relevant to nanomaterials processing operations.

Conflict of Interest

There are no conflicts of interest. This article does not include research in which human participants were involved. Informed consent not applicable. This article does not include any research in which animal participants were involved.

Data Availability Statement

The datasets generated and supporting the findings of this article are obtainable from the corresponding author upon reasonable request.

References

[1] Vajravelu, K., and Mukhopadhyay, S., 2016, *Fluid Flow, Heat and Mass Transfer at Bodies of Different Shapes: Numerical Solutions*, Elsevier, New York.
[2] Sakiadis, B. C., 1961, "Boundary-Layer Behavior on Continuous Solid Surfaces: I. Boundary-Layer Equations for Two-Dimensional and Axisymmetric Flow," AIChE J., **7**(1), pp. 26–28.
[3] Sakiadis, B. C., 1961, "Boundary-Layer Behavior on Continuous Solid Surfaces: II. The Boundary Layer on a Continuous Flat Surface," AIChE J., **7**(2), pp. 221–225.
[4] Crane, L. J., 1970, "Flow Past a Stretching Plate," Z. Angew. Math. Phys., **21**(4), pp. 645–647.
[5] Liancun, Z., Lijuan, W., and Xinxin, Z., 2011, "Analysis Solutions of Unsteady Flow and Heat Transfer on a Permeable Stretching Sheet With Non-Uniform Heat Source/Sink," Commun. Nonlinear Sci. Numer. Simul., **16**(2), pp. 731–740.
[6] Anwar Bég, O., Bakier, A. Y., and Prasad, V. R., 2009, "Numerical Study of Free Convection Magnetohydrodynamic Heat and Mass Transfer From a Stretching Surface to a Saturated Porous Medium With Soret and Dufour Effects," Comput. Mater. Sci., **46**(1), pp. 57–65.
[7] Anwar Bég, O., Zueco, J., and Takhar, H. S., 2008, "Laminar Free Convection From a Continuously Moving Vertical Surface in a Thermally Stratified, Non-Darcian High-Porosity Medium: Network Numerical Study," Int. Commun. Heat Mass Transfer, **35**(7), pp. 810–816.
[8] Gupta, D., Kumar, L., Bég, O. A., and Singh, B., 2015, "Finite Element Simulation of Nonlinear Magneto-Micropolar Stagnation Point Flow From a Porous Stretching Sheet With Prescribed Skin Friction," Comput. Therm. Sci., **7**(1), pp. 1–14.
[9] Ishak, A., Nazar, R., and Pop, I., 2006, "Mixed Convection Boundary Layers in the Stagnation Point Flow Towards a Stretching Vertical Sheet," Meccanica, **41**(5), pp. 509–518.
[10] Anwar Bég, O., Bhargava, R., Sharma, S., Kadir, A., Bég, T. A., and Shamshuddin, M., 2020, "Numerical Solutions for Axisymmetric Non-Newtonian Stagnation Enrobing Flow, Heat and Mass Transfer With Application to Cylindrical Pipe Coating Dynamics," Comput. Therm. Sci., In Press.
[11] Ramesh, G. K., Gireesha, B. J., and Bagewadi, C. S., 2012, "MHD Flow of a Dusty Fluid Near the Stagnation Point Over a Permeable Stretching Sheet With Non-Uniform Source/Sink," Int. J. Heat Mass Transfer, **55**(17–18), pp. 4900–4907.
[12] Mehmood, R., Rana, S., Anwar Bég, O., and Kadir, A., 2019, "Numerical Study of Chemical Reaction Effects in Magnetohydrodynamic Oldroyd-B Oblique Stagnation Flow With a Non-Fourier Heat Flux Model," J. Braz. Soc. Mech. Sci. Eng., **40**(11), pp. 1–14.
[13] Das, S. K., Choi, S. U., Yu, W., and Pradeep, T., 2007, *Nanofluids: Science and Technology*, John Wiley & Sons, Hoboken, NJ.
[14] Anwar Bég, O., 2018, "Chapter 5: Nonlinear Multi-Physical Laminar Nanofluid Bioconvection Flows: Models and Computation," *Computational Approaches in Biomedical Nano-Engineering*, A Sohail, and Z Li, eds., Wiley, New York, pp. 113–145.
[15] Choi, S., and Eastman, J., 1995, "Enhancing Thermal Conductivity of Fluids With Nanoparticles," 1995 ASME International Mechanical Engineering Congress and Exposition, San Francisco, CA, Nov. 12–17, pp. 99–105.
[16] Choi, S. U. S., Zhang, Z. G., Yu, W., Lockwood, F. E., and Grulke, E. A., 2001, "Anomalous Thermal Conductivity Enhancement in Nanotube Suspensions," Appl. Phys. Lett., **79**(14), pp. 2252–2254.
[17] Masuda, H., Ebata, A., Teramea, K., and Hishinuma, N., 1993, "Alteration of Thermal Conductivity and Viscosity of Liquid by Dispersing Ultra-Fine Particles," Netsu Bussei, **4**(4), pp. 227–233.
[18] Das, S. K., Putra, N., Thiesen, P., and Roetzel, W., 2003, "Temperature Dependence of Thermal Conductivity Enhancement for Nanofluids," ASME J. Heat Transfer-Trans. ASME, **125**(4), pp. 567–574.
[19] Pak, B. C., and Cho, Y. I., 1998, "Hydrodynamic and Heat Transfer Study of Dispersed Fluids With Submicron Metallic Oxide Particles," Exp. Heat Transfer, **11**(2), pp. 151–170.
[20] Xuan, Y., and Li, Q., 2003, "Investigation on Convective Heat Transfer and Flow Features of Nanofluids," ASME J. Heat Transfer-Trans. ASME, **125**(1), pp. 151–155.
[21] Eastman, J. A., Choi, S. U. S., Li, S., Yu, W., and Thompson, L. J., 2001, "Anomalously Increased Effective Thermal Conductivities of Ethylene Glycol-Based Nanofluids Containing Copper Nanoparticles," Appl. Phys. Lett., **78**(6), pp. 718–720.
[22] Mintsa, H. A., Roy, G., Nguyen, C. T., and Doucet, D., 2009, "New Temperature Dependent Thermal Conductivity Data for Water-Based Nanofluids," Int. J. Therm. Sci., **48**(2), pp. 363–371.

[23] Trisaksri, V., and Wongwises, S., 2007, "Critical Review of Heat Transfer Characteristics of Nanofluids," Renewable Sustainable Energy Rev., **11**(3), pp. 512–523.
[24] Wang, X.-Q., and Mujumdar, A. S., 2007, "Heat Transfer Characteristics of Nanofluids: A Review," Inter. J. Therm. Sci., **46**(1), pp. 1–19.
[25] Eastman, J., Phillpot, S., Choi, S., and Keblinski, P., 2004, "Thermal Transport in Nanofluids," Annu. Rev. Mater. Res., **34**(1), pp. 219–246.
[26] Kakaç, S., and Pramuanjaroenkij, A., 2009, "Review of Convective Heat Transfer Enhancement With Nanofluids," Int. J. Heat Mass Transfer, **52**(13–14), pp. 3187–3196.
[27] Maré, T., Halelfadl, S., Sow, O., Estellé, P., Duret, S., and Bazantay, F., 2011, "Comparison of the Thermal Performances of Two Nanofluids at Low Temperature in a Plate Heat Exchanger," Exp. Therm. Fluid Sci., **35**(8), pp. 1535–1543.
[28] Liu, M. S., Ching-Cheng Lin, M., Huang, I. T., and Wang, C. C., 2005, "Enhancement of Thermal Conductivity With Carbon Nanotube for Nanofluids," Int. Commun. Heat Mass Transfer, **32**(9), pp. 1202–1210.
[29] Garg, P., Alvarado, J. L., Marsh, C., Carlson, T. A., Kessler, D. A., and Annamalai, K., 2009, "An Experimental Study on the Effect of Ultrasonication on Viscosity and Heat Transfer Performance of Multi-Wall Carbon Nanotube-Based Aqueous Nanofluids," Int. J. Heat Mass Transfer, **52**(21–22), pp. 5090–5101.
[30] Xue, Q. Z., 2005, "Model for Thermal Conductivity of Carbon Nanotube-Based Composites," Phys. B Condens. Matter, **368**(1–4), pp. 302–307.
[31] Ding, Y., Alias, H., Wen, D., and Williams, R. A., 2006, "Heat Transfer of Aqueous Suspensions of Carbon Nanotubes (CNT Nanofluids)," Int. J. Heat Mass Transfer, **49**(1–2), pp. 240–250.
[32] Sharma, T., Mohanareddy, A., Chandra, T., and Ramaprabhu, S., 2008, "Development of Carbon Nanotubes and Nanofluids Based Microbial Fuel Cell," Int. J. Hydrogen Energy, **33**(22), pp. 6749–6754.
[33] Kamali, R., and Binesh, A., 2010, "Numerical Investigation of Heat Transfer Enhancement Using Carbon Nanotube-Based Non-Newtonian Nanofluids," Int. Commun. Heat Mass Transfer, **37**(8), pp. 1153–1157.
[34] Khan, W. A., Khan, Z. H., and Rahi, M., 2014, "Fluid Flow and Heat Transfer of Carbon Nanotubes Along a Flat Plate With Navier Slip Boundary," Appl. Nanosci., **4**(5), pp. 633–641.
[35] Sher Akbar, N., Raza, M., and Ellahi, R., 2015, "Influence of Induced Magnetic Field and Heat Flux With the Suspension of Carbon Nanotubes for the Peristaltic Flow in a Permeable Channel," J. Magn. Magn. Mater., **381**, pp. 405–415.
[36] Khan, W. A., Culham, R., and Haq, R. U., 2015, "Heat Transfer Analysis of MHD Water Functionalized Carbon Nanotube Flow Over a Static/Moving Wedge," J. Nanomater., **2015**, pp. 1–13.
[37] Kumaresan, V., Velraj, R., and Das, S. K., 2012, "Convective Heat Transfer Characteristics of Secondary Refrigerant-Based CNT Nanofluids in a Tubular Heat Exchanger," Int. J. Refrig., **35**(8), pp. 2287–2296.
[38] Sharma, R. K., Ganesan, P., Tyagi, V. V., Metselaar, H. S. C., and Sandaran, S. C., 2015, "Developments in Organic Solid–Liquid Phase Change Materials and Their Applications in Thermal Energy Storage," Energy Convers. Manage., **95**, pp. 193–228.
[39] Shalaby, S. M., and Bek, M. A., 2014, "Experimental Investigation of a Novel Indirect Solar Dryer Implementing PCM as Energy Storage Medium," Energy Convers. Manage., **83**, pp. 1–8.
[40] Zhang, P., Meng, Z. N., Zhu, H., Wang, Y. L., and Peng, S. P., 2017, "Melting Heat Transfer Characteristics of a Composite Phase Change Material Fabricated by Paraffin and Metal Foam," Appl. Energy, **185**, pp. 1971–1983.
[41] Bachok, N., Ishak, A., and Pop, I., 2010, "Melting Heat Transfer in Boundary Layer Stagnation-Point Flow Towards a Stretching Sheet/Shrinking Sheet," Phys. Lett. A, **374**(40), pp. 4075–4079.
[42] Viswanath, R., and Jaluria, Y. A., 1993, "Comparison of Different Solution Methodologies for Melting and Solidification Problems in Enclosures," Numer. Heat Transf. B: Fundam., **24**(1), pp. 77–105.
[43] Prescott, P. J., and Incropera, F. P., 1996, "Convection Heat and Mass Transfer in Alloy Solidification," Adv. Heat Transfer, **28**, pp. 231–338.
[44] Jaluria, Y., 1992, "Transport From Continuously Moving Materials Undergoing Thermal Processing," Annu. Rev. Fluid Mech., **4**(4), pp. 187–245.
[45] Venkatadri, K., Abdul Gaffar, S., Suryanarayana Reddy, M., Ramachandra Prasad, V., Khan, B., and Anwar Bég, O., 2020, "Melting Heat Transfer Analysis on Magnetohydrodynamics Buoyancy Convection in an Enclosure: A Numerical Study," J. Appl. Comput. Mech., **6**(1), pp. 52–62.
[46] Gupta, D., Kumar, L., Anwar Bég, O., and Singh, B., 2019, "Finite Element Analysis of Melting Effects on MHD Stagnation-Point Non-Newtonian Flow and Heat Transfer From a Stretching/Shrinking Sheet, Emerging Trends in Mathematical Sciences and Its Applications," AIP Conf. Proc., **2061**, p. 020024.
[47] Amirsom, N. A., Basir, M. F. M., Uddin, M. J., Ismail, A. I., Anwar Bég, O., and Kadir, A., 2019, "Computation of Melting Dissipative Magnetohydrodynamic Nanofluid Bioconvection With Second Order Slip and Variable Thermophysical Properties," Appl. Sci., **9**(12), pp. 1–22.
[48] Muhammad, K., Hayat, T., Alsaedi, A., and Ahmad, B., 2020, "Melting Heat Transfer in Squeezing Flow of Basefluid (Water), Nanofluid (CNTs + Water) and Hybrid Nanofluid (CNTs + CuO + Water)," J. Therm. Anal. Calorim., **143**(2), pp. 1157–1174.
[49] Hayat, T., Muhammad, K., Farooq, M., and Alsaedi, A., 2016, "Melting Heat Transfer in Stagnation Point Flow of Carbon Nanotubes Towards Variable Thickness Surface," AIP Adv., **6**(1), p. 015214.
[50] Chen, Y., and Zheng, Q., 2018, "A Novel CNT Encapsulated Phase Change Material With Enhanced Thermal Conductivity and Photo-Thermal Conversion Performance," Sol. Energy Mater Sol. Cells, **184**, pp. 82–90.
[51] Ryglowski, B. K., Pollak, R. D., and Kwon, Y. W., 2010, "Characterizing the Stability of Carbon Nanotube-Enhanced Water as a Phase Change Material for Thermal Management Systems," ASME J. Thermal Sci. Eng. Appl., **2**(4), p. 041007.
[52] Anwar Bég, O., Uddin, M. J., Bég, T. A., Kadir, A., Shamshuddin, M., and Babaie, M., 2019, "Modelling Mass Transfer From a Rotating Cone in Anisotropic Porous Media With Stefan Blowing and Navier Slip," Indian J. Phys., **94**(6), pp. 863–877.
[53] Reddy, N. V. B., Kishan, N., and Reddy, C. S., 2019, "Melting Heat Transfer and MHD Boundary Layer Flow of Eyring-Powell Nanofluid Over a Nonlinear Stretching Sheet With Slip," Int. J. Appl. Mech. Eng., **24**(1), pp. 10–20.
[54] Hone, J., Llaguno, M. C., Biercuk, M. J., Johnson, A. T., Batlogg, B., Benes, Z., and Fischer, J. E., 2002, "Thermal Properties of Carbon Nanotubes and Nanotube-Based Material," Appl. Phys. A, **74**(3), pp. 339–343.
[55] Antar, Z., Noel, H., Feller, J. F., Glouannec, P., and Elleuch, K., 2012, "Thermophysical and Radiative Properties of Conductive Biopolymer Composite," Matter. Sci. Forum, **714**, pp. 115–122.
[56] Kierzenka, J., and Shampine, L. F., 2001, "A BVP Solver Based on Residual Control and the MATLAB PSE," ACM Trans. Math. Softw., **27**(3), pp. 299–316.
[57] Wang, C. Y., 2008, "Stagnation Flow Towards a Shrinking Sheet," Int. J. Non Linear Mech., **43**(5), pp. 377–382.
[58] Kimiaeifar, A., Bagheri, G. H., Rahimpour, M., and Mehrabian, M. A., 2009, "Analytical Solution of a Two-Dimensional Stagnation Flow in the Vicinity of a Shrinking Sheet by Means of the Homotopy Analysis Method," Proc. Inst. Mech. Eng. Part E J. Process Mech. Eng., **223**(3), pp. 133–143.
[59] Mehmood, R., Tabassum, R., Kuharat, S., Anwar Bég, O., and Babaie, M., 2019, "Thermal Slip in Oblique Radiative Nano-Polymer Gel Transport With Temperature-Dependent Viscosity: Solar Collector Nanomaterial Coating Manufacturing Simulation," Arabian J. Sci. Eng., **44**(2), pp. 1525–1541.